

# AutoRefiner: Improving Autoregressive Video Diffusion Models via Reflective Refinement over the Stochastic Sampling Path

Zhengyang Yu<sup>†,\*</sup> Akio Hayakawa<sup>‡</sup> Masato Ishii<sup>‡</sup> Qingtao Yu<sup>†</sup>

Takashi Shibuya<sup>‡</sup> Jing Zhang<sup>†</sup>, Yuki Mitsufuji<sup>‡,§</sup>

<sup>†</sup> Australian National University <sup>‡</sup>Sony AI <sup>§</sup>Sony Group Corporation

{zhengyang.yu, terry.yu, jing.zhang}@anu.edu.au

{akio.hayakawa, masato.a.ishii, takashi.tak.shibuya, yuhki.mitsufuji}@sony.com



Figure 1. *AutoRefiner* efficiently enhances base AR-VDMs through feedforward refinement of noises sampled along the intermediate denoising path, achieving improved video fidelity across aspects such as perceptual quality and scene–motion alignment with text input.

## Abstract

Autoregressive video diffusion models (AR-VDMs) show strong promise as scalable alternatives to bidirectional VDMs, enabling real-time and interactive applications. Yet there remains room for improvement in their sample fidelity. A promising solution is inference-time alignment, which optimizes the noise space to improve sample fidelity without updating model parameters. Yet, optimization- or search-based methods are computationally impractical for AR-VDMs. Recent text-to-image (T2I) works address this via feedforward noise refiners that modulate sampled noises in a single forward pass. **Can such noise refiners be extended to AR-VDMs?** We identify the failure of naïvely extending T2I noise refiners to AR-VDMs and propose AutoRefiner—a

noise refiner tailored for AR-VDMs, with two key designs: pathwise noise refinement and a reflective KV-cache. Experiments demonstrate that AutoRefiner serves as an efficient plug-in for AR-VDMs, effectively enhancing sample fidelity by refining noise along stochastic denoising paths.

## 1. Introduction

Recent advances in video diffusion models (VDMs) enabled photorealistic and temporally coherent video synthesis [11, 12, 27, 68]. However, most VDMs employ bidirectional temporal attention, generating all frames jointly without respecting causal order, which limits their use in real-time or interactive applications. Autoregressive video diffusion models (AR-VDMs) [9, 32, 88] have emerged as a promising alternative, which condition on previously generated frames to predict future ones, forming the foundation

\*Work done during an internship at Sony AI

for applications such as neural game engines [13, 15], cinematic creation [80, 93], and world simulation [50, 50, 81]. Yet, there remains substantial room to improve the sample fidelity of AR-VDMs, e.g., maintaining high perceptual fidelity, realistic motion dynamics, and semantic alignment. While scaling model capacity and data have been the dominant route to improving sample fidelity of diffusion models, a rapidly growing orthogonal direction focuses on improving generation capacity at inference time. This line of work, known as *inference-time alignment* [70], enhances sample fidelity or optimizes specific reward functions at inference time without fine-tuning the base model. The core idea is to exploit the stochasticity inherent in the noise sampling process of diffusion models. Existing methods identify “golden noises” either by optimizing noise as a learnable latent via reward gradients [3, 18, 59], or by searching for noise samples that yield higher reward scores [22, 35, 46, 51]. While both strategies have proven effective for text-to-image (T2I) models, applying them to AR-VDMs is computationally impractical: optimization-based methods require costly gradient propagation through multiple denoising steps—easily leading to out-of-memory issues for large VDMs—whereas search-based methods demand over hundreds of trials per generation, with computational cost further scaling with the temporal rollout length of AR-VDMs.

We therefore consider a more practical objective—learning a feedforward network for AR-VDMs that directly maps a random noise to its locally optimized counterpart in a single forward pass, which we call a **noise refiner**, achieving a similar effect to inference-time alignment with only minor degradation in inference efficiency. While the similar idea of a noise refiner has been explored in T2I works [1, 19, 94], we observe that their naïve extension to AR-VDMs yields only moderate or worse performance and reward hacking issues. We attribute the culprit to refining the *initial* noise, a design suited to deterministic samplers. Such a strategy fails for step-distilled AR-VDMs that rely on stochastic sampling to maintain sample fidelity (Fig. 3), where the intermediate stochasticity dilutes the influence of the initial noise. We additionally observe that initial noise refinement is prone to reward hacking issues such as motion degradation and ‘grid-like’ artifacts (Fig. 7).

To address these limitations, we introduce *AutoRefiner*—the first noise refinement framework tailored for AR-VDMs. The failure of initial noise refinement and the critical role of intermediate noises in the sampling process with AR-VDMs motivate our design of **pathwise noise refinement**, which refines the noises sampled along the intermediate denoising path rather than the initial noise. Built upon the base AR-VDM and trained via efficient LoRA [30] fine-tuning, *AutoRefiner* naturally inherits the base model’s autoregressive architecture, enabling it to leverage the KV cache for temporal conditioning. We extend this capabil-

ity with a **reflective KV-cache** mechanism, allowing the refiner to condition on both historical frames and the previous denoising state. This design equips *AutoRefiner* with a context-aware and self-reflection ability to identify locally optimized noises more effectively. Our contributions are:

1. We identify and analyze the failure of T2I noise refiners when extended to AR-VDMs.
2. We propose *AutoRefiner*, a noise refinement framework for AR-VDMs featuring pathwise noise refinement and a reflective KV cache mechanism that jointly enables context-aware noise refinement along the denoising path.
3. We demonstrate that *AutoRefiner* serves as a plugin that improves the performance of two mainstream AR-VDM paradigms—Diffusion-Forcing [9] and Self-Forcing [32] without incurring costly inference.

## 2. Related Work

**Bidirectional VDMs.** Building on the success of image diffusion models [4, 17, 47, 53, 56, 57], video diffusion models (VDMs) generalize diffusion models to synthesize temporally coherent and high-fidelity videos. These include pixel-space models [26, 27, 60, 89] and latent-space models [11, 12, 20, 21, 23, 28, 67, 68, 71, 72, 74, 86].

**AR VDMs.** The temporal continuity of videos naturally lends itself to a next-frame prediction scheme for video generation. Rolling Diffusion [92] and its variants [37, 39, 43, 66, 82, 90] adopt a sliding-window denoising strategy. However, these methods depend on overlapping windows to mitigate error accumulation, leading to substantial latency. Inspired by the success of LLMs [6], recent works explore hybrid diffusion-AR training schemes. Diffusion Forcing (DF) [9] and its extensions [10, 62, 69, 88] train VDMs with independently sampled per-frame noise levels, enabling next-frame denoising during inference conditioned on clean past frames. CausVid [88] employs DF to train causal few-step VDMs via step-distillation [87] from a bidirectional teacher. Self-Forcing (SF) [32] and its variants [14, 43, 85] address the train-test discrepancy of DF by simulating rollouts during training, improving extrapolative consistency and alleviating exposure bias [58].

**Diffusion Inference-Time Alignment.** Similar to the inference-time scaling behavior observed in LLMs [5, 61], recent studies [35, 46, 49, 51, 84] have shown that scaling compute to search for “golden noises” during inference can substantially enhance diffusion sampling quality. Another line of work [18, 59] iteratively optimizes noise with differentiable reward models [38, 75, 79, 83], improving human preference alignment or controllability. While these works achieve notable quality gains, they often incur substantial computational overhead. Recent efforts have proposed training noise refiners [1, 19, 94] that directly predict optimized input noise in a single forward pass, removing the need for costly search or optimization at inference time.

### 3. Method

#### 3.1. Preliminaries: Autoregressive VDMs

**Next-chunk Prediction by Autoregression.** An autoregressive video diffusion model is a hybrid framework that approximates the joint distribution of temporally ordered video frames or chunks. Given a video sequence of length  $N$ , denoted as  $\mathbf{x}^{1:N} = (\mathbf{x}^1, \mathbf{x}^2, \dots, \mathbf{x}^N)$ , the joint distribution can be factorized into a product of conditionals  $p(\mathbf{x}^{1:N}) = \prod_{i=1}^N p(\mathbf{x}^i | \mathbf{x}^{<i})$ . Each conditional  $p(\mathbf{x}^i | \mathbf{x}^{<i})$  is approximated by a denoising model  $G_\theta$

$$\mathbf{x}^i = f_{\theta, t_1} \circ f_{\theta, t_2} \circ \dots \circ f_{\theta, t_T} (\mathbf{x}_{t_T}^i) \sim q_\theta (\mathbf{x}^i | \mathbf{x}^{<i}), \quad (1)$$

where  $\mathbf{x}_{t_T}^i \sim \mathcal{N}(0, I)$  is the input noise, and  $\{t_0 = 0, t_1, \dots, t_T = T_{\max}\}$  is a subsequence of timesteps  $[0, \dots, T_{\max}]$ .  $f_{\theta, t_j}$  is an intermediate stochastic sampling step involving denoising followed by renoising [87]:

$$f_{\theta, t_j} (\mathbf{x}_{t_j}^i) = \Psi (\mathbf{x}_{0|t_j}^i, \epsilon_{t_j}^i, t_{j-1}), \quad (2)$$

where the denoising step is defined as

$$\mathbf{x}_{0|t_j}^i = G_\theta (\Psi (\mathbf{x}_{0|t_{j+1}}^i, \epsilon_{t_j}^i, t_j); \mathbf{x}^{<i}, t_j), \quad (3)$$

which denoises noisy input latents  $\mathbf{x}_{t_j}^i$  conditioned on clean historical frame chunks  $\mathbf{x}^{<i}$ . Here, we omit the text condition of the denoising model for brevity. The intermediate path noise  $\epsilon_{t_{j-1}}^i \sim \mathcal{N}(0, I)$  is then sampled to introduce stochasticity and renoise the sample to the next timestep through the forward diffusion process [25, 42, 44]

$$\Psi (\mathbf{x}, \epsilon_{t_j}, t_j) = \alpha_{t_j} \mathbf{x} + \sigma_{t_j} \epsilon_{t_j}, \quad (4)$$

where  $\alpha_{t_j}$  and  $\sigma_{t_j}$  follow a predefined noise schedule over timestep  $t$  [42]. Such a renoising process is crucial to maintain sample fidelity of AR-VDMs (explained in Sec. 3.3).

**Step Distillation.** To achieve real-time responsiveness in streaming applications, the denoising model  $G_\theta$  is typically step-distilled from a multi-step teacher model, allowing valid sampling with a small number of diffusion steps  $T$ . We mainly consider the state-of-the-art AR-VDM paradigm—Self-Forcing (SF) [32]. Unlike Teacher Forcing [40] or Diffusion Forcing [9], which condition on ground-truth history frames, SF conditions on self-rollout frames during training, thereby eliminating the train–test distribution gap. The history conditioning is achieved through causal attention and KV cache [32, 88]. The self-rollout strategy further enables holistic optimization by directly evaluating the fidelity of generated clean videos, rather than relying on local score matching or flow matching. This is accomplished via the DMD loss [87]

$$\nabla_\theta \mathcal{L}_{\text{DMD}} = \mathbb{E}_t (\nabla_\theta \text{KL} (q_{\theta, t} (\mathbf{x}^{1:N}) \| p_t (\mathbf{x}^{1:N}))), \quad (5)$$

which approximates the gradient of the inverse KL divergence between the model and target data distributions.

#### 3.2. Learning Framework of AutoRefiner

Given a pre-trained AR-VDM  $G_\theta$  and a differentiable scorer  $R$  that measures video fidelity, our objective is to improve the sample quality of  $G_\theta$  by steering its base distribution  $q_\theta$  towards a tilted distribution

$$q_\theta^* (\mathbf{x}^{1:N}) \propto q_\theta (\mathbf{x}^{1:N}) \exp (R (\mathbf{x}^{1:N})), \quad (6)$$

that better aligns  $R$ . In practice,  $R$  can be instantiated in various forms, such as a distributional scorer like DMD loss in Eq. (5) or a human preference scorer [75, 79, 83]. To achieve this, rather than directly updating the base model parameters, we leverage the stochasticity [2, 63] inherent in the stochastic sampling steps of Eq. (1). Given the set of sampled noises, each rollout step from the conditional in Eq. (1) can be interpreted as a deterministic mapping from the sampled initial and intermediate noises to the output video chunk as follows

$$\mathbf{x}^i = F_\theta (\mathbf{x}_{t_T}^i, \epsilon^i; \mathbf{x}^{<i}) \sim q_\theta (\mathbf{x}^i | \mathbf{x}^{<i}), \quad (7)$$

where  $F_\theta$  denotes the composition of all denoising steps parameterized by  $G_\theta$ . Recent works show that the sampled noises in the diffusion process are not created equal [46, 51]. Given the same diffusion model, generation quality can be significantly improved by carefully selecting the noise samples. Inspired by these findings, we aim to learn the tilted distribution  $q_\theta^* (\mathbf{x}^{1:N})$  by transforming randomly sampled noises along the intermediate denoising path

$$\epsilon^{i*} = \arg \max_{\epsilon^i} (R (F_\theta (\mathbf{x}_{t_T}^i, \epsilon^i; \mathbf{x}^{<i})) - \text{Reg} (\epsilon^i)), \quad (8)$$

where  $\epsilon^i \sim \mathcal{N}(0, I)$ ,  $\text{Reg} (\epsilon^i)$  is a regularization term that keeps the transformed noise close to the original one. Eq. (8) can be solved by per-sample noise optimization [18] or searching [46]. However, with a noise candidate number or optimization step of  $L$ , such methods have a time complexity of  $O(TLN)$ . Given that  $L$  is usually hundreds or even thousands of steps, this is impractical for AR-VDMs, especially for real-time applications. Instead, we adopt the idea of *noise refiners* [1, 19, 94]. Specifically, we parameterize a feedforward network  $T_\phi$  that learns to map a randomly sampled noise  $\epsilon_{t_j}^i$  to an optimized one  $\hat{\epsilon}_{t_j}^i = \epsilon_{t_j}^i + \Delta \epsilon_{t_j}^i$  with the following objective

$$\mathcal{L}(\phi) = \mathbb{E}_{i, \epsilon^i, j} \left[ R (\mathbf{x}_{0|t_j}^i) - \frac{1}{2} \|\Delta \epsilon_{t_j}^i\|^2 \right], \quad (9)$$

where the random noise  $\epsilon_{t_j}^i$  is refined by a predicted residual term from  $T_\phi$  that conditions on both the clean history frames  $\mathbf{x}^{<i}$  and the denoising output from the previous

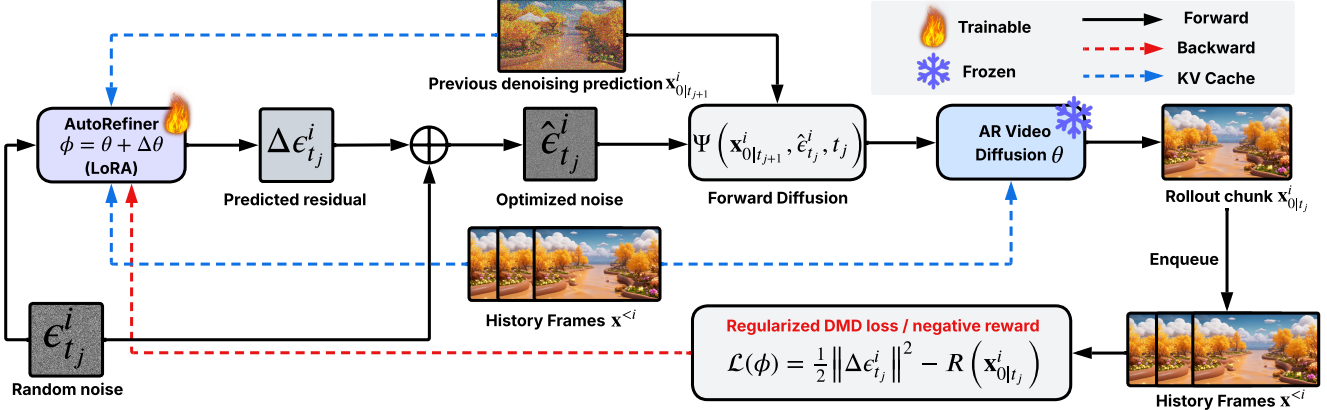


Figure 2. **The AutoRefiner method.** *AutoRefiner* is a feed-forward plug-in network for enhancing pretrained AR-VDMs. Without modifying the base model parameters, it is trained to maximize distribution-matching or reward-based video-fidelity scores by refining randomly sampled noises along the intermediate denoising trajectory (Sec. 3.3). Built through LoRA fine-tuning, *AutoRefiner* inherits the autoregressive structure of the base AR-VDM and extends its KV cache mechanism to a reflective KV cache (Fig. 4), allowing it to condition on both historical frames and the previous denoising prediction for more effective, context-aware noise refinement (Sec. 3.4).

timestep  $\mathbf{x}_{0|t_j}^i$ , i.e.,  $\Delta\epsilon_{t_j}^i = T_\phi(\epsilon_{t_j}^i; \mathbf{x}_{0|t_{j+1}}^i, \mathbf{x}^{<i})$ . Following the denoising step in Eq. (3), the interpolation between the refined noise  $\hat{\epsilon}_{t_j}^i$  and the denoising output from the previous timestep  $\mathbf{x}_{0|t_{j+1}}^i$  is used as input to obtain the current-timestep denoising prediction via

$$\mathbf{x}_{0|t_j}^i = G_\theta(\Psi(\mathbf{x}_{0|t_{j+1}}^i, \hat{\epsilon}_{t_j}^i); \mathbf{x}^{<i}, t_j), \quad (10)$$

for which the fidelity score  $R(\mathbf{x}_{0|t_j}^i)$  is computed. The  $L_2$  term approximates the KL divergence between the modified noise distribution and the original Gaussian distribution [19], which regularizes the refined noise to remain Gaussian distributed and ensures that the tilted distribution can maintain the sample diversity of the base model.

### 3.3. From Initial to Pathwise Noise Refinement

The learning framework in Sec. 3.2 fundamentally differs from prior T2I noise refiners [1, 19, 94] with one crucial distinction: it refines the noise sequence  $\{\epsilon_{1:T-1}^i\}$  sampled from the intermediate path, rather than the initial noise  $\mathbf{x}_{t_T}^i$ . We next elaborate on the rationale behind this design.

**Limitation of Initial Noise Refinement.** We first investigate the effect of applying the refiner to the initial noise space of AR-VDMs, following the design of prior text-to-image noise refiners [1, 19, 94]. Empirically, this strategy yields limited or unstable performance for AR-VDMs. Depending on the choice of the differentiable fidelity scorer  $R$ , we observe two distinct failure behaviors:

- **With distribution matching loss.** When  $R$  is instantiated as the DMD loss [87], refining the initial noise  $\mathbf{x}_{t_T}^i$  yields moderate or worse performance (Tab. 1). This finding contrasts with prior work that reports substantial improvements from optimization in the initial noise space for T2I

diffusion models. We conjecture that this discrepancy arises from differences in sampling strategies. Earlier approaches typically adopt ODE-based samplers, where the initial noise constitutes the sole source of stochasticity; thus, optimizing it can yield inference-scaling behavior [46]. In contrast, step-distilled AR-VDMs depend on stochastic sampling during few-step inference [64, 87], as expressed in Eq. (2), where randomness is reintroduced at intermediate steps. The injection of such intermediate noise introduces additional randomness, which dilutes the influence of initial noise optimization. Consequently, optimizing the initial noise alone cannot reliably steer overall sample quality, as later stochastic perturbations partially overwrite the effects of the refined initialization.

- **With preference-based reward scores.** In contrast, when  $R$  is instantiated as a preference-based reward scorer—aimed at improving perceptual quality and semantic alignment, we observe reward hacking behaviors such as motion degradation and grid-like artifacts (see Fig. 7 and supplementary). We conjecture that this arises because the initial noise determines the low-frequency components of the generated video, which the refiner can easily exploit to obtain higher reward scores by taking shortcuts, e.g., the modified initial noise  $\hat{\mathbf{x}}_{t_T}^i$  can strongly influence the overall motion magnitude of the sample [7, 8], enabling the refiner to trivially reconstructing the previous chunk, i.e.,  $F_\theta(\hat{\mathbf{x}}_{t_T}^i, \epsilon^i; \mathbf{x}^{<i}) \approx \mathbf{x}^{i-1}$ . This shortcut increases the reward by producing static frames with minimal motion blur (see low motion degree in Tab. 2 and examples in supplementary), rather than genuinely improving the quality of generated videos.

**Pathwise Noise Refinement.** Given the limitations of initial noise refinement, we instead train  $T_\phi$  with a differ-



Figure 3. Replacing the stochastic sampler of Self-Forcing with an ODE sampler leads to over-saturation and drifting artifacts.

---

#### Algorithm 1 Training algorithm of *AutoRefiner*

---

**Require:** Denoising timesteps  $\{t_1, \dots, t_T\}$ . Number of training video chunks  $N$ . Pre-trained AR-VDM  $G_\theta$ . Differentiable fidelity scorer  $R$ .

```

1: Initialize noise refiner  $T_\phi(\cdot) = \mathbf{0}$  via LoRA on  $G_\theta$ 
2: while training do
3:   Initialize output  $\mathbf{X} \leftarrow []$ ,  $\mathcal{L}_{\text{reg}} \leftarrow 0$ .
4:   Sample  $s \sim \text{Uniform}(1, 2, \dots, T-1)$ 
5:   for  $i = 1, \dots, N$  do
6:     Disable gradient computation
7:     Initialize  $\mathbf{x}_{t_T}^i \sim \mathcal{N}(0, \mathbf{I})$ 
8:      $\mathbf{x}_{0|t_T}^i \leftarrow G_\theta(\mathbf{x}_{t_T}^i; t_T, \mathbf{X})$ 
9:     for  $j = T-1, \dots, s$  do
10:      Enable gradient computation if  $j = s$ 
11:      Sample  $\epsilon_{t_j}^i \sim \mathcal{N}(0, \mathbf{I})$ 
12:       $\Delta\epsilon_{t_j}^i \leftarrow T_\phi(\epsilon_{t_j}^i; \mathbf{x}_{0|t_{j+1}}^i, \mathbf{X})$ 
13:       $\mathbf{x}_{t_j}^i \leftarrow \Psi(\mathbf{x}_{0|t_{j+1}}^i, \epsilon_{t_j}^i + \Delta\epsilon_{t_j}^i, t_j)$ 
14:       $\mathbf{x}_{0|t_j}^i \leftarrow G_\theta(\mathbf{x}_{t_j}^i; t_j, \mathbf{X})$ 
15:       $\mathbf{X}.\text{append}(\mathbf{x}_{0|t_s}^i)$ 
16:       $\mathcal{L}_{\text{reg}} \leftarrow \mathcal{L}_{\text{reg}} + \frac{1}{2} \|\Delta\epsilon_{t_j}^i\|^2$ 
17:   Gradient step on  $-\nabla_\phi(R(\mathbf{X}) - \mathcal{L}_{\text{reg}})$ 

```

---

ent objective than previous methods: *refinement along the stochastic sampling path*. Unlike prior T2I noise refiners that optimize the initial noise  $\mathbf{x}_{t_T}^i$ , our formulation in Eq. (9) changes the refinement target to the intermediate noise sequence  $\epsilon_{t_{1:T-1}}^i$ . As shown in Fig. 3, removing the stochasticity introduced by intermediate noises—by replacing the stochastic sampler with an ODE sampler—results in color saturation and drifting artifacts, underscoring its crucial role in preserving the fidelity of generated samples in AR-VDMs. Since intermediate noises perturb the denoised output from the previous timestep via the forward diffusion process Eq. (4), we conjecture that they act as a self-correction mechanism [34], injecting stochasticity to correct errors accumulated from earlier steps. Our learning framework in Sec. 3.2 leverages this property by training  $T_\phi$  to steer the denoising path towards higher fidelity modes.

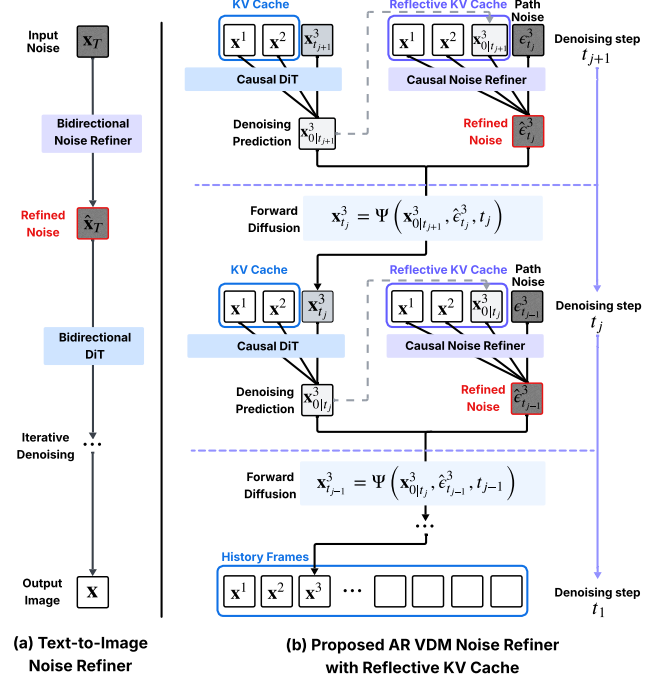


Figure 4. Illustration of the difference between existing T2I noise refiners and *AutoRefiner*. In contrast to prior text-to-image (T2I) noise refiners that operate on the initial noise space, *AutoRefiner* performs refinement along the intermediate denoising trajectory. Equipped with a **reflective KV cache**, *AutoRefiner* conditions each noise refinement step on both historical frames and the denoised latent from the previous diffusion timestep.

### 3.4. AR Noise Refiner with Reflective KV Cache

**Noise Refiner Network.** We initialize  $T_\phi$  by the pre-trained autoregressive VDM  $G_\theta$  to leverage its powerful prior knowledge. We train the refiner via LoRA [30] adapters, which reduces memory overhead and avoids creating a separate copy for the base model. Following Eyring et al. [19], we modify both the final layer weight and bias parameters of the base model to zero, which ensures that the initial output residual of  $T_\phi$  is zero. This stabilizes training during the early iterations and prevents divergence.

**Reflective KV Cache.** One fundamental advantage of autoregressive models is their ability to memorize past states via KV cache, allowing the models to predict future states based on their own previous predictions. We extend this capability to the autoregressive noise refiner  $T_\phi$  with a reflective KV cache mechanism, which enables each prediction step of  $T_\phi$  to condition on a richer context beyond the text-only conditioning used in prior T2I noise refiners. This includes two primary components. First, it inherits the conditioning on predicted history frames  $\mathbf{x}^{<i}$  from the base AR-VDM, ensuring that noise modulation does not destroy the overall temporal consistency. At the same time, this con-

ditioning enables  $T_\phi$  to enhance motion quality when optimized with a temporal fidelity scorer. Moreover, it also conditions on the denoising output from the previous timestep  $\mathbf{x}_{0|t_{j+1}}^i$ , which also serves as the latent to be perturbed by the modulated noise through  $\Psi(\mathbf{x}_{0|t_{j+1}}^i, \hat{\epsilon}_{t_j}^i, t_j)$ . By conditioning on  $\mathbf{x}_{0|t_{j+1}}^i$ ,  $T_\phi$  can refine intermediate path noises to correct errors or undesired artifacts present in  $\mathbf{x}_{0|t_{j+1}}^i$  that have accumulated from previous denoising steps. This process functions analogously to self-reflection [54], wherein the model “looks back” at its prior decisions to identify and rectify earlier mistakes. Conditioning on the reflective KV cache,  $T_\phi$  takes in a randomly sampled intermediate path noise  $\epsilon_{t_j}^i$  as input, with which the regularized optimization objective in Eq. (9) encourages the refiner to identify a locally optimal noise around  $\epsilon_{t_j}^i$ , avoiding distribution shift and preserving the stochasticity of the base model  $G_\theta$ , which is conceptually similar to the first-order noise search [46]. To establish a consistent correspondence between each refined noise frame and its associated denoised latent, we apply the same Rotary Position Encoding (RoPE) [65] to both  $\epsilon_{t_j}^i$  and  $\mathbf{x}_{0|t_{j+1}}^i$ .

**Efficient Optimization.** Although  $G_\theta$  is step-distilled, few-step sampling still incurs significant memory overhead due to maintaining the computational graph of the denoising chain  $f_{\theta, t_1} \circ f_{\theta, t_2} \circ \dots \circ f_{\theta, t_{T-1}}$ . To address this, as shown in Algorithm 1, we adopt a similar gradient truncation strategy from Huang et al. [32], which restricts backpropagation to a single, randomly selected final noise refinement step  $t_s$ , where  $s \sim \text{Uniform}(1, 2, \dots, T-1)$ . We additionally detach the gradient flow from the predicted history frames and previous denoising output through the reflective KV cache.

## 4. Experiments

In this section, we validate the performance of *AutoRefiner* and the effect of the proposed components through quantitative and qualitative evaluations with three perspectives:

- *Q1.* Does *AutoRefiner* enhance the general generative capability of base AR-VDMs when trained with a generative distribution matching loss?
- *Q2.* Can *AutoRefiner* improve specific preference dimensions when trained with reward-based objectives?
- *Q3.* Demonstrate the effectiveness of the proposed path-wise noise refinement and reflective KV cache.

**Datasets.** The training of the proposed method does not require any video data. We adopt the VidProS subset from VidProM [73] as the training prompt dataset, which is filtered and preprocessed by Huang et al. [32]. For evaluation, we use 946 prompts from VBench [33]. Please refer to supplementary for further implementation details.

	Num Params ↓	Total Score ↑	Quality Score ↑	Semantic Score. ↑
<b>Self-Forcing</b> [32]	1.3B	84.05	84.93	80.54
+LoRA	1.4B	82.10	82.65	79.93
+InitNoiseRefiner	1.4B	83.76	84.63	80.29
<b>+AutoRefiner (ours)</b>	1.4B	<b>84.72</b>	<b>85.41</b>	<b>81.95</b>
<b>CausVid</b> [88]	1.3B	83.06	84.24	78.35
+LoRA	1.4B	83.43	84.74	78.18
+InitNoiseRefiner	1.4B	82.23	83.13	78.64
<b>+AutoRefiner (ours)</b>	1.4B	<b>83.84</b>	<b>84.82</b>	<b>79.93</b>

Table 1. Comparison with baseline methods using distribution-matching distillation (DMD Eq. (5)) loss as the training objective. We compare our approach against baseline methods using overall video fidelity scores from VBench (best result in **bold**).

### 4.1. Experiments with DMD-based Training

For our experimental setup to answer *Q1*, we train *AutoRefiner* using the Distribution Matching Distillation (DMD) loss [87] as defined in Eq. (5), and assess its effect on the general generative capability of the base AR-VDMs. Since the base AR-VDMs are already optimized with the DMD loss, we train *AutoRefiner* as a plug-in module to further reduce the gap between generated and real data distributions.

**Evaluation Metric.** Since this setting targets improving general video generation capability, we report overall video fidelity scores averaged across all VBench [33] dimensions.

**Baselines.** We consider the following baselines:

- **Baseline AR-VDMs.** We consider two most representative AR-VDMs as baselines—**Self-Forcing** [32] and **CausVid** [88] (based on Diffusion-Forcing [9]). *AutoRefiner* is served as a plug-in noise refiner to both models.
- **Fine-tuning methods.** We also compare with fine-tuning via **LoRA** and an initial-timestep noise refiner (**InitNoiseRefiner**) variant that trains a noise refiner for only the initial noise  $\mathbf{x}_{t_T}^i$ , which follows the similar implementation of Eyring et al. [19] for T2I models.

**Results.** Tab. 1 shows the quantitative results on overall VBench scores. For Self-Forcing, LoRA degrades performance, indicating that simply adding more parameters through fine-tuning does not improve generation fidelity. Likewise, InitNoiseRefiner fails to yield the performance gains observed in prior T2I works. In contrast, *AutoRefiner* improves both overall quality and semantic scores, as also evidenced qualitatively in Fig. 5. For CausVid, LoRA degrades textual alignment—e.g., incorrect camera motion in Fig. 5 (left) and an incorrect number of objects in Fig. 5 (right), while the initial noise refiner lowers visual quality (Tab. 1). In contrast, *AutoRefiner* achieves clear gains for both dimensions. As shown in Fig. 6, CausVid tends to exhibit over-saturation as more frames are generated. We conjecture that the cause is due to compounding errors accumulated during rollout. *AutoRefiner* reduces such artifacts and improves the overall cross-frame consistency.

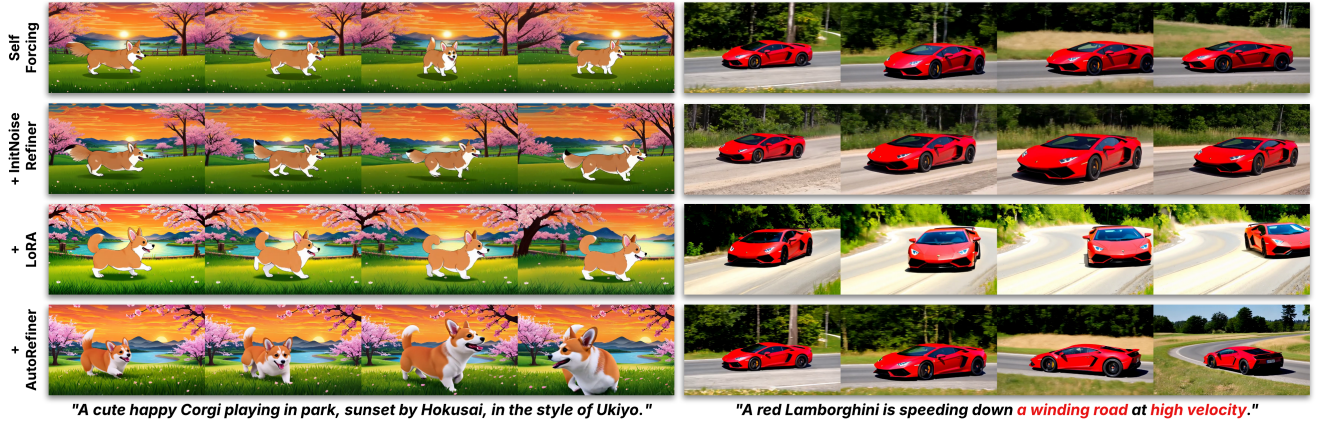


Figure 5. Qualitative comparison with baselines on training with DMD loss, using Self-Forcing [32] as the base model. Compared to the baselines, *AutoRefiner* shows improved visual fidelity (as illustrated by the higher visual quality of the ‘corgi’ example), and motion alignment with text prompt (as shown by the faithfully reflected winding road and high velocity in the ‘car’ example).

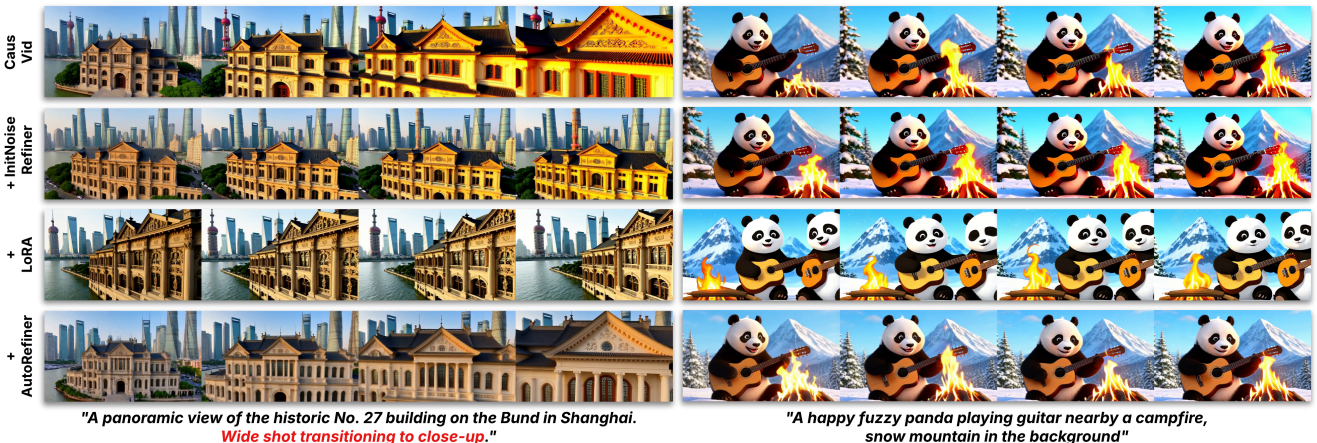


Figure 6. Qualitative comparison with baselines on training with DMD loss, using CausVid [88] as the base model. *AutoRefiner* alleviates the cross-frame inconsistency issue of CausVid, as observed in the gradually saturated color of the “building” (left) and the “sky” (right).

## 4.2. Experiments with Reward-based Training

To evaluate *Q2*, we train *AutoRefiner* using a combination of reward models following Li et al. [41]: two image reward models—HPSv2.1 [79], which captures human preference, and CLIPScore [52], which measures frame-level text alignment, and a video reward model—InternVideo2 [76], which measures spatiotemporal consistency with text prompts. Under this setting, *AutoRefiner* is trained to steer the pre-trained AR-VDMs toward preference dimensions emphasizing perceptual quality and semantic alignment.

**Evaluation Metric.** In accordance with the dimensions emphasized by reward models, we evaluate performance on eight metrics from VBench focusing on (1) *perceptual quality* (imaging and aesthetic quality; motion degree and style) and (2) *semantic alignment* (textual alignment measured by Tag2Text [31] and ViClip [75]; object class accuracy for both single- and multi-object generation). We also report

the introduced inference-time computational overhead relative to the base model, including additional NFE ( $\Delta$ NFE), reward verification (#Verify), VAE decoding ( $\Delta$ VAE), and the resulting frames-per-second (FPS). **Baselines.** We use Self-Forcing as the base model under this setting. In addition to LoRA and InitNoiseRefiner introduced in Sec. 4.1, we further compare against two searching-based inference-time alignment methods adapted from text-to-image works such as Ma et al. [46]:

- **Best-of-N (BoN).** Randomly samples 5 initial noise candidates for each video chunk and selects the one achieving the highest reward score as output.
- **Search-over-Path (SoP).** Samples five noise candidates at each initial and intermediate timestep, choosing after every step the denoised output with the highest reward to serve as the input to the next timestep.

**Results.** The quantitative results of reward-based training



Figure 7. Qualitative comparison with baselines on training with reward scores. *AutoRefiner* improves perceptual quality (left example) and temporal coherence (right example), without suffering from reward hacking issues observed in LoRA and initial noise refiner.

Method	Compute Overhead				Visual Quality↑		Motion Quality↑		Textual Alignment↑		Object Accuracy↑	
	$\Delta NFE \downarrow$	#Verify $\downarrow$	$\Delta VAE \downarrow$	FPS $\uparrow$	Imaging	Aesthetic	Degree	Style	Tag2Text	ViClip	Single	Multi
Self-Forcing [32]	-	-	-	10.3	69.24	65.78	<b>69.44</b>	24.58	52.83	26.80	94.22	88.41
+ BoN	112	5	4	2.48	68.76	66.03	63.89	24.59	<b>60.68</b>	<b>27.13</b>	92.41	<b>91.84</b>
+ SoP	112	20	19	1.22	68.77	66.03	63.89	<b>24.60</b>	<b>60.47</b>	<b>27.14</b>	92.48	<b>91.62</b>
+ LoRA	0	0	0	9.48	<b>74.52</b>	<b>67.30</b>	0.00	22.76	50.73	26.12	<b>94.78</b>	82.62
+ InitNoiseRefiner	7	0	0	7.57	70.76	66.04	30.56	24.40	54.00	26.70	<b>94.94</b>	83.08
+ AutoRefiner (ours)	21	0	0	6.32	<b>70.89</b>	<b>66.26</b>	<b>79.17</b>	<b>24.68</b>	57.63	26.94	94.62	91.23

Table 2. Comparison with baseline methods using reward models as objective/guidance, the **best** and **second best** results are highlighted.

are shown in Tab. 2. *AutoRefiner* consistently improves Self-Forcing across all evaluation dimensions, indicating effective alignment with the reward models—also reflected in the improved perceptual quality and motion coherence in Fig. 7. Both LoRA and InitNoiseRefiner exhibit clear reward hacking behaviors with severely degraded motion degree and visual artifacts such as grid patterns (InitNoiseRefiner) or cartoonish textures (LoRA). Although BoN and SoP achieve noticeable gains in semantic alignment, they incur substantial computational overhead, whereas *AutoRefiner* requires considerably less inference computation.

### 4.3. Ablation studies

**Ablation on Refined Timesteps.** We conduct an ablation over different intermediate refinement timesteps  $\{750, 500, 250\}$  to analyze the contribution of each timestep. We consider two settings: (1) refining a single timestep, and (2) omitting one of the three intermediate timesteps. The results are shown in Tab. 3. We observe: (1) earlier timesteps contribute more to performance gains. We conjecture that this is because the denoising prediction  $\mathbf{x}_{0|t_j}^i$  at earlier timesteps has lower sample fidelity, which leaves the noise refiner more room for correction; (2) omitting any step leads to a degradation in performance. Based on these findings, we apply noise refinement for all three intermediate denoising steps.

Refined Timesteps			Quality Score $\uparrow$	Semantic Score $\uparrow$	Total Score $\uparrow$
750	500	250			
✓	✗	✗	85.34	81.68	84.61
✗	✓	✗	85.17	81.53	84.43
✗	✗	✓	85.16	81.32	84.40
✗	✓	✓	85.15	81.76	84.48
✓	✗	✓	85.33	81.73	84.61
✓	✓	✗	85.21	81.72	84.51
✓	✓	✓	<b>85.41</b>	<b>81.95</b>	<b>84.72</b>

Table 3. Ablation on diffusion timesteps used for refinement.

KV cache form		Quality Score $\uparrow$	Semantic Score $\uparrow$	Total Score $\uparrow$
History	Denoised			
✗	✗	85.13	81.35	84.37
✗	✓	85.11	81.57	84.41
✓	✗	85.17	81.24	84.39
✓	✓	<b>85.41</b>	<b>81.95</b>	<b>84.72</b>

Table 4. Ablation on different KV cache mechanisms.

**Ablation on KV Cache Mechanisms.** We ablate the proposed reflective KV cache mechanism (Sec. 3.4) by selectively removing its two conditioning components: the history frames  $\mathbf{x}^{<i}$ , the denoised output from the previous timestep  $\mathbf{x}_{0|t_{j+1}}^i$ . We find that incorporating both conditions yields the best performance, validating our design choice.

## 5. Conclusion

We introduced *AutoRefiner*, an efficient noise refinement framework for AR-VDMs. Unlike prior T2I refiners that operate on initial noise, *AutoRefiner* performs pathwise refinement along the denoising trajectory and integrates a reflective KV-cache to leverage temporal and contextual cues. Across both distributional and reward-based objectives, *AutoRefiner* consistently improves sample fidelity, motion quality, and semantic alignment of base AR-VDMs. We hope this work inspires future research on efficient inference-time alignment for improved video generation.

## References

- [1] Donghoon Ahn, Jiwon Kang, Sanghyun Lee, Jaewon Min, Minjae Kim, Wooseok Jang, Hyoungwon Cho, Sayak Paul, SeonHwa Kim, Eunju Cha, et al. A noise is worth diffusion guidance. *arXiv preprint arXiv:2412.03895*, 2024. [2](#), [3](#), [4](#)
- [2] Brian DO Anderson. Reverse-time diffusion equation models. *Stochastic Processes and their Applications*, 12(3):313–326, 1982. [3](#)
- [3] Heli Ben-Hamu, Omri Puny, Itai Gat, Brian Karrer, Uriel Singer, and Yaron Lipman. D-flow: Differentiating through flows for controlled generation, 2024. [2](#)
- [4] Black-Forest. Flux. <https://blackforestlabs.ai/announcing-black-forest-labs/>, 2024. [2](#)
- [5] Bradley Brown, Jordan Juravsky, Ryan Ehrlich, Ronald Clark, Quoc V Le, Christopher Ré, and Azalia Mirhoseini. Large language monkeys: Scaling inference compute with repeated sampling. *arXiv preprint arXiv:2407.21787*, 2024. [2](#)
- [6] Tom Brown, Benjamin Mann, Nick Ryder, Melanie Subbiah, Jared D Kaplan, Prafulla Dhariwal, Arvind Neelakantan, Pranav Shyam, Girish Sastry, Amanda Askell, et al. Language models are few-shot learners. In *NeurIPS*, pages 1877–1901, 2020. [2](#)
- [7] Ryan Burgert, Yuancheng Xu, Wenqi Xian, Oliver Pilarski, Pascal Clausen, Mingming He, Li Ma, Yitong Deng, Lingxiao Li, Mohsen Mousavi, et al. Go-with-the-flow: Motion-controllable video diffusion models using real-time warped noise. In *Proceedings of the Computer Vision and Pattern Recognition Conference*, pages 13–23, 2025. [4](#)
- [8] Pascal Chang, Jingwei Tang, Markus Gross, and Vinius C Azevedo. How i warped your noise: a temporally-correlated noise prior for diffusion models. *arXiv preprint arXiv:2504.03072*, 2025. [4](#)
- [9] Boyuan Chen, Diego Martí Monsó, Yilun Du, Max Simchowitz, Russ Tedrake, and Vincent Sitzmann. Diffusion forcing: Next-token prediction meets full-sequence diffusion. *Advances in Neural Information Processing Systems*, 37:24081–24125, 2024. [1](#), [2](#), [3](#), [6](#)
- [10] Guibin Chen, Dixuan Lin, Jiangping Yang, Chunze Lin, Junchen Zhu, Mingyuan Fan, Hao Zhang, Sheng Chen, Zheng Chen, Chengcheng Ma, et al. Skyreels-v2: Infinite-length film generative model. *arXiv preprint arXiv:2504.13074*, 2025. [2](#)
- [11] Haoxin Chen, Menghan Xia, Yingqing He, Yong Zhang, Xiaodong Cun, Shaoshu Yang, Jinbo Xing, Yaofang Liu, Qifeng Chen, Xintao Wang, et al. Videocrafter1: Open diffusion models for high-quality video generation. *arXiv preprint arXiv:2310.19512*, 2023. [1](#), [2](#)
- [12] Haoxin Chen, Yong Zhang, Xiaodong Cun, Menghan Xia, Xintao Wang, Chao Weng, and Ying Shan. Videocrafter2: Overcoming data limitations for high-quality video diffusion models. In *Proceedings of the IEEE/CVF Conference on Computer Vision and Pattern Recognition*, pages 7310–7320, 2024. [1](#), [2](#)
- [13] Xinle Cheng, Tianyu He, Jiayi Xu, Junliang Guo, Di He, and Jiang Bian. Playing with transformer at 30+ fps via next-frame diffusion. *arXiv preprint arXiv:2506.01380*, 2025. [2](#)
- [14] Justin Cui, Jie Wu, Ming Li, Tao Yang, Xiaojie Li, Rui Wang, Andrew Bai, Yuanhao Ban, and Cho-Jui Hsieh. Self-forcing++: Towards minute-scale high-quality video generation. *arXiv preprint arXiv:2510.02283*, 2025. [2](#)
- [15] Julian Decart, Julian Quevedo, Quinn McIntyre, Spruce Campbell, Xinlei Chen, and Robert Wachen. Oasis: A universe in a transformer. <https://oasis-model.github.io/>, 2024. [2](#)
- [16] Bradley Efron. Tweedie’s formula and selection bias. *Journal of the American Statistical Association*, 106(496):1602–1614, 2011. [1](#)
- [17] Patrick Esser, Sumith Kulal, Andreas Blattmann, Rahim Entezari, Jonas Müller, Harry Saini, Yam Levi, Dominik Lorenz, Axel Sauer, Frederic Boesel, et al. Scaling rectified flow transformers for high-resolution image synthesis. In *Forty-first International Conference on Machine Learning*, 2024. [2](#)
- [18] Luca Eyring, Shyamgopal Karthik, Karsten Roth, Alexey Dosovitskiy, and Zeynep Akata. Reno: Enhancing one-step text-to-image models through reward-based noise optimization. *Advances in Neural Information Processing Systems*, 37:125487–125519, 2024. [2](#), [3](#)
- [19] Luca Eyring, Shyamgopal Karthik, Alexey Dosovitskiy, Nataniel Ruiz, and Zeynep Akata. Noise hypernetworks: Amortizing test-time compute in diffusion models. *arXiv preprint arXiv:2508.09968*, 2025. [2](#), [3](#), [4](#), [5](#), [6](#)
- [20] genmo. mochi. <https://www.genmo.ai/blog>, 2024. [2](#)
- [21] Yuwei Guo, Ceyuan Yang, Anyi Rao, Zhengyang Liang, Yaohui Wang, Yu Qiao, Maneesh Agrawala, Dahua Lin, and Bo Dai. Animatediff: Animate your personalized text-to-image diffusion models without specific tuning. *arXiv preprint arXiv:2307.04725*, 2023. [2](#)
- [22] Yingqing Guo, Yukang Yang, Hui Yuan, and Mengdi Wang. Training-free guidance beyond differentiability: Scalable path steering with tree search in diffusion and flow models, 2025. [2](#)
- [23] Yingqing He, Tianyu Yang, Yong Zhang, Ying Shan, and Qifeng Chen. Latent video diffusion models for high-fidelity long video generation. *arXiv preprint arXiv:2211.13221*, 2022. [2](#)
- [24] Jonathan Ho and Tim Salimans. Classifier-free diffusion guidance. *CoRR*, abs/2207.12598, 2022. [2](#)

[25] Jonathan Ho, Ajay Jain, and Pieter Abbeel. Denoising diffusion probabilistic models. In *NeurIPS*, pages 6840–6851, 2020. 3

[26] Jonathan Ho, William Chan, Chitwan Saharia, Jay Whang, Ruiqi Gao, Alexey Gritsenko, Diederik P Kingma, Ben Poole, Mohammad Norouzi, David J Fleet, et al. Imagen video: High definition video generation with diffusion models. *arXiv preprint arXiv:2210.02303*, 2022. 2

[27] Jonathan Ho, Tim Salimans, Alexey Gritsenko, William Chan, Mohammad Norouzi, and David J Fleet. Video diffusion models. *Advances in Neural Information Processing Systems*, 35:8633–8646, 2022. 1, 2

[28] Wenyi Hong, Ming Ding, Wendi Zheng, Xinghan Liu, and Jie Tang. Cogvideo: Large-scale pretraining for text-to-video generation via transformers. *arXiv preprint arXiv:2205.15868*, 2022. 2

[29] Alain Hore and Djemel Ziou. Image quality metrics: Psnr vs. ssim. In *2010 20th international conference on pattern recognition*, pages 2366–2369. IEEE, 2010. 2

[30] Edward J. Hu, Yelong Shen, Phillip Wallis, Zeyuan Allen-Zhu, Yuanzhi Li, Shean Wang, Lu Wang, and Weizhu Chen. Lora: Low-rank adaptation of large language models. In *ICLR*. OpenReview.net, 2022. 2, 5

[31] Xinyu Huang, Youcai Zhang, Jinyu Ma, Weiwei Tian, Rui Feng, Yuejie Zhang, Yaqian Li, Yandong Guo, and Lei Zhang. Tag2text: Guiding vision-language model via image tagging. *arXiv preprint arXiv:2303.05657*, 2023. 7

[32] Xun Huang, Zhengqi Li, Guande He, Mingyuan Zhou, and Eli Shechtman. Self forcing: Bridging the train-test gap in autoregressive video diffusion. *arXiv preprint arXiv:2506.08009*, 2025. 1, 2, 3, 6, 7, 8, 4

[33] Ziqi Huang, Yinan He, Jiahuo Yu, Fan Zhang, Chenyang Si, Yuming Jiang, Yuanhan Zhang, Tianxing Wu, Qingyang Jin, Nattapol Chanpaisit, et al. Vbench: Comprehensive benchmark suite for video generative models. In *Proceedings of the IEEE/CVF Conference on Computer Vision and Pattern Recognition*, pages 21807–21818, 2024. 6

[34] Tero Karras, Miika Aittala, Timo Aila, and Samuli Laine. Elucidating the design space of diffusion-based generative models. *Advances in Neural Information Processing Systems*, 35:26565–26577, 2022. 5

[35] Shyamgopal Karthik, Karsten Roth, Massimiliano Mancini, and Zeynep Akata. If at first you don't succeed, try, try again: Faithful diffusion-based text-to-image generation by selection. *arXiv preprint arXiv:2305.13308*, 2023. 2

[36] Dongjun Kim, Chieh-Hsin Lai, Wei-Hsiang Liao, Naoki Murata, Yuhta Takida, Toshimitsu Uesaka, Yutong He, Yuki Mitsufuji, and Stefano Ermon. Consistency trajectory models: Learning probability flow ode trajectory of diffusion. *arXiv preprint arXiv:2310.02279*, 2023. 3

[37] Jihwan Kim, Junoh Kang, Jinyoung Choi, and Bohyung Han. Fifo-diffusion: Generating infinite videos from text without training. *Advances in Neural Information Processing Systems*, 37:89834–89868, 2024. 2

[38] Yuval Kirstain, Adam Polyak, Uriel Singer, Shahbuland Matiana, Joe Penna, and Omer Levy. Pick-a-pic: An open dataset of user preferences for text-to-image generation. *Advances in neural information processing systems*, 36:36652–36663, 2023. 2

[39] Akio Kodaira, Tingbo Hou, Ji Hou, Masayoshi Tomizuka, and Yue Zhao. Streamdit: Real-time streaming text-to-video generation. *arXiv preprint arXiv:2507.03745*, 2025. 2

[40] Alex M Lamb, Anirudh Goyal ALIAS PARTH GOYAL, Ying Zhang, Saizheng Zhang, Aaron C Courville, and Yoshua Bengio. Professor forcing: A new algorithm for training recurrent networks. *Advances in neural information processing systems*, 29, 2016. 3

[41] Jiachen Li, Qian Long, Jian Zheng, Xiaofeng Gao, Robinson Piramuthu, Wenhui Chen, and William Yang Wang. T2v-turbo-v2: Enhancing video generation model post-training through data, reward, and conditional guidance design. *arXiv preprint arXiv:2410.05677*, 2024. 7

[42] Yaron Lipman, Ricky TQ Chen, Heli Ben-Hamu, Maximilian Nickel, and Matt Le. Flow matching for generative modeling. *arXiv preprint arXiv:2210.02747*, 2022. 3, 1

[43] Kunhao Liu, Wenbo Hu, Jiale Xu, Ying Shan, and Shijian Lu. Rolling forcing: Autoregressive long video diffusion in real time. *arXiv preprint arXiv:2509.25161*, 2025. 2

[44] Xingchao Liu, Chengyue Gong, and Qiang Liu. Flow straight and fast: Learning to generate and transfer data with rectified flow. *arXiv preprint arXiv:2209.03003*, 2022. 3, 1

[45] Ilya Loshchilov and Frank Hutter. Decoupled weight decay regularization. *arXiv preprint arXiv:1711.05101*, 2017. 1

[46] Nanye Ma, Shangyuan Tong, Haolin Jia, Hexiang Hu, Yu-Chuan Su, Mingda Zhang, Xuan Yang, Yandong Li, Tommi Jaakkola, Xuhui Jia, et al. Inference-time scaling for diffusion models beyond scaling denoising steps. *arXiv preprint arXiv:2501.09732*, 2025. 2, 3, 4, 6, 7

[47] Alexander Quinn Nichol, Prafulla Dhariwal, Aditya Ramesh, Pranav Shyam, Pamela Mishkin, Bob McGrew, Ilya Sutskever, and Mark Chen. GLIDE: towards photorealistic image generation and editing with text-guided diffusion models. In *ICML*, pages 16784–16804. PMLR, 2022. 2

[48] Maxime Oquab, Timothée Darcet, Théo Moutakanni, Huy Vo, Marc Szafraniec, Vasil Khalidov, Pierre Fernandez, Daniel Haziza, Francisco Massa, Alaaeldin El-Nouby, et al. Dinov2: Learning robust visual features without supervision. *arXiv preprint arXiv:2304.07193*, 2023. 2

[49] Yuta Oshima, Masahiro Suzuki, Yutaka Matsuo, and Hiroki Furuta. Inference-time text-to-video alignment with diffusion latent beam search. *arXiv preprint arXiv:2501.19252*, 2025. 2

[50] Ryan Po, Yotam Nitzan, Richard Zhang, Berlin Chen, Tri Dao, Eli Shechtman, Gordon Wetzstein, and Xun Huang. Long-context state-space video world models. *arXiv preprint arXiv:2505.20171*, 2025. 2

[51] Zipeng Qi, Lichen Bai, Haoyi Xiong, and Zeke Xie. Not all noises are created equally: Diffusion noise selection and optimization. *arXiv preprint arXiv:2407.14041*, 2024. 2, 3

[52] Alec Radford, Jong Wook Kim, Chris Hallacy, Aditya Ramesh, Gabriel Goh, Sandhini Agarwal, Girish Sastry, Amanda Askell, Pamela Mishkin, Jack Clark, et al. Learning transferable visual models from natural language supervision. In *ICML*, pages 8748–8763. PMLR, 2021. 7

[53] Aditya Ramesh, Prafulla Dhariwal, Alex Nichol, Casey Chu, and Mark Chen. Hierarchical text-conditional image generation with clip latents. *arXiv preprint arXiv:2204.06125*, 1(2):3, 2022. 2

[54] Matthew Renze and Erhan Guven. Self-reflection in llm agents: Effects on problem-solving performance. *arXiv preprint arXiv:2405.06682*, 2024. 6

[55] Herbert E Robbins. An empirical bayes approach to statistics. In *Breakthroughs in Statistics: Foundations and basic theory*, pages 388–394. Springer, 1992. 1

[56] Robin Rombach, Andreas Blattmann, Dominik Lorenz, Patrick Esser, and Björn Ommer. High-resolution image synthesis with latent diffusion models. In *Proceedings of the IEEE/CVF conference on computer vision and pattern recognition*, pages 10684–10695, 2022. 2

[57] Chitwan Saharia, William Chan, Saurabh Saxena, Lala Li, Jay Whang, Emily L Denton, Kamyar Ghasemipour, Raphael Gontijo Lopes, Burcu Karagol Ayan, Tim Salimans, et al. Photorealistic text-to-image diffusion models with deep language understanding. In *NeurIPS*, 2022. 2

[58] Florian Schmidt. Generalization in generation: A closer look at exposure bias. *arXiv preprint arXiv:1910.00292*, 2019. 2

[59] Christian Simon, Masato Ishii, Akio Hayakawa, Zhi Zhong, Shusuke Takahashi, Takashi Shibuya, and Yuki Mitsu-fuji. Titan-guide: Taming inference-time alignment for guided text-to-video diffusion models. *arXiv preprint arXiv:2508.00289*, 2025. 2

[60] Uriel Singer, Adam Polyak, Thomas Hayes, Xi Yin, Jie An, Songyang Zhang, Qiyuan Hu, Harry Yang, Oron Ashual, Oran Gafni, et al. Make-a-video: Text-to-video generation without text-video data. *arXiv preprint arXiv:2209.14792*, 2022. 2

[61] Charlie Snell, Jaehoon Lee, Kelvin Xu, and Aviral Kumar. Scaling llm test-time compute optimally can be more effective than scaling model parameters. *arXiv preprint arXiv:2408.03314*, 2024. 2

[62] Kiwhan Song, Boyuan Chen, Max Simchowitz, Yilun Du, Russ Tedrake, and Vincent Sitzmann. History-guided video diffusion. *arXiv preprint arXiv:2502.06764*, 2025. 2

[63] Yang Song, Jascha Sohl-Dickstein, Diederik P. Kingma, Abhishek Kumar, Stefano Ermon, and Ben Poole. Score-based generative modeling through stochastic differential equations. In *ICLR*. OpenReview.net, 2021. 3

[64] Yang Song, Prafulla Dhariwal, Mark Chen, and Ilya Sutskever. Consistency models. 2023. 4, 3

[65] Jianlin Su, Murtadha Ahmed, Yu Lu, Shengfeng Pan, Wen Bo, and Yunfeng Liu. Roformer: Enhanced transformer with rotary position embedding. *Neurocomputing*, 568:127063, 2024. 6

[66] Mingzhen Sun, Weining Wang, Gen Li, Jiawei Liu, Jiahui Sun, Wanquan Feng, Shanshan Lao, SiYu Zhou, Qian He, and Jing Liu. Ar-diffusion: Asynchronous video generation with auto-regressive diffusion. In *Proceedings of the Computer Vision and Pattern Recognition Conference*, pages 7364–7373, 2025. 2

[67] HPC-AI Tech. Open-sora. <https://github.com/hpcatech/Open-Sora>, 2024. 2

[68] tencent. hunyuan. <https://aivideo.hunyuan.tencent.com/>, 2024. 1, 2

[69] Hansi Teng, Hongyu Jia, Lei Sun, Lingzhi Li, Maolin Li, Mingqiu Tang, Shuai Han, Tianning Zhang, WQ Zhang, Weifeng Luo, et al. Magi-1: Autoregressive video generation at scale. *arXiv preprint arXiv:2505.13211*, 2025. 2

[70] Masatoshi Uehara, Yulai Zhao, Chenyu Wang, Xiner Li, Aviv Regev, Sergey Levine, and Tommaso Biancalani. Inference-time alignment in diffusion models with reward-guided generation: Tutorial and review. *arXiv preprint arXiv:2501.09685*, 2025. 2

[71] Team Wan, Ang Wang, Baole Ai, Bin Wen, Chaojie Mao, Chen-Wei Xie, Di Chen, Feiwu Yu, Haiming Zhao, Jianxiao Yang, et al. Wan: Open and advanced large-scale video generative models. *arXiv preprint arXiv:2503.20314*, 2025. 2, 1

[72] Jiuniu Wang, Hangjie Yuan, Dayou Chen, Yingya Zhang, Xiang Wang, and Shiwei Zhang. Modelscope text-to-video technical report, 2023. 2

[73] Wenhao Wang and Yi Yang. Vidprom: A million-scale real prompt-gallery dataset for text-to-video diffusion models. *Advances in Neural Information Processing Systems*, 37: 65618–65642, 2024. 6

[74] Yaohui Wang, Xinyuan Chen, Xin Ma, Shangchen Zhou, Ziqi Huang, Yi Wang, Ceyuan Yang, Yinan He, Jiashuo Yu, Peiqing Yang, et al. Lavie: High-quality video generation with cascaded latent diffusion models. *arXiv preprint arXiv:2309.15103*, 2023. 2

[75] Yi Wang, Yinan He, Yizhuo Li, Kunchang Li, Jiashuo Yu, Xin Ma, Xinhao Li, Guo Chen, Xinyuan Chen, Yaohui Wang, et al. Internvid: A large-scale video-text dataset for multimodal understanding and generation. *arXiv preprint arXiv:2307.06942*, 2023. 2, 3, 7

[76] Yi Wang, Kunchang Li, Xinhao Li, Jiashuo Yu, Yinan He, Guo Chen, Baoqi Pei, Rongkun Zheng, Zun Wang, Yansong Shi, et al. Internvideo2: Scaling foundation models for multimodal video understanding. In *European Conference on Computer Vision*, pages 396–416. Springer, 2024. 7

[77] Zhou Wang, Alan C Bovik, Hamid R Sheikh, and Eero P Simoncelli. Image quality assessment: from error visibility to structural similarity. *IEEE transactions on image processing*, 13(4):600–612, 2004. 2

[78] Zhengyi Wang, Cheng Lu, Yikai Wang, Fan Bao, Chongxuan Li, Hang Su, and Jun Zhu. Prolificdreamer: High-fidelity and diverse text-to-3d generation with variational score distillation. *arXiv preprint arXiv:2305.16213*, 2023. 1

[79] Xiaoshi Wu, Yiming Hao, Keqiang Sun, Yixiong Chen, Feng Zhu, Rui Zhao, and Hongsheng Li. Human preference score v2: A solid benchmark for evaluating human preferences of text-to-image synthesis. *arXiv preprint arXiv:2306.09341*, 2023. 2, 3, 7

[80] Junfei Xiao, Ceyuan Yang, Lvmin Zhang, Shengqu Cai, Yang Zhao, Yuwei Guo, Gordon Wetzstein, Maneesh Agrawala, Alan Yuille, and Lu Jiang. Captain cinema: Towards short movie generation. *arXiv preprint arXiv:2507.18634*, 2025. 2

[81] Zeqi Xiao, Yushi Lan, Yifan Zhou, Wenqi Ouyang, Shuai Yang, Yanhong Zeng, and Xingang Pan. Worldmem: Long-term consistent world simulation with memory. *arXiv preprint arXiv:2504.12369*, 2025. 2

[82] Desai Xie, Zhan Xu, Yicong Hong, Hao Tan, Difan Liu, Feng Liu, Arie Kaufman, and Yang Zhou. Progressive autoregressive video diffusion models. In *Proceedings of the Computer Vision and Pattern Recognition Conference*, pages 6322–6332, 2025. 2

[83] Jiazheng Xu, Xiao Liu, Yuchen Wu, Yuxuan Tong, Qinkai Li, Ming Ding, Jie Tang, and Yuxiao Dong. Imageward: Learning and evaluating human preferences for text-to-image generation. *Advances in Neural Information Processing Systems*, 36:15903–15935, 2023. 2, 3

[84] Haolin Yang, Feilong Tang, Ming Hu, Qingyu Yin, Yulong Li, Yexin Liu, Zelin Peng, Peng Gao, Junjun He, Zongyuan Ge, et al. Scalingnoise: Scaling inference-time search for generating infinite videos. *arXiv preprint arXiv:2503.16400*, 2025. 2

[85] Shuai Yang, Wei Huang, Ruihang Chu, Yicheng Xiao, Yuyang Zhao, Xianbang Wang, Muyang Li, Enze Xie, Yingcong Chen, Yao Lu, et al. Longlive: Real-time interactive long video generation. *arXiv preprint arXiv:2509.22622*, 2025. 2

[86] Zhuoyi Yang, Jiayan Teng, Wendi Zheng, Ming Ding, Shiyu Huang, Jiazheng Xu, Yuanming Yang, Wenyi Hong, Xiaohan Zhang, Guanyu Feng, et al. Cogvideox: Text-to-video diffusion models with an expert transformer. *arXiv preprint arXiv:2408.06072*, 2024. 2

[87] Tianwei Yin, Michaël Gharbi, Richard Zhang, Eli Shechtman, Fredo Durand, William T Freeman, and Taesung Park. One-step diffusion with distribution matching distillation. In *Proceedings of the IEEE/CVF conference on computer vision and pattern recognition*, pages 6613–6623, 2024. 2, 3, 4, 6, 1

[88] Tianwei Yin, Qiang Zhang, Richard Zhang, William T Freeman, Fredo Durand, Eli Shechtman, and Xun Huang. From slow bidirectional to fast autoregressive video diffusion models. In *Proceedings of the Computer Vision and Pattern Recognition Conference*, pages 22963–22974, 2025. 1, 2, 3, 6, 7, 4

[89] David Junhao Zhang, Jay Zhangjie Wu, Jia-Wei Liu, Rui Zhao, Lingmin Ran, Yuchao Gu, Difei Gao, and Mike Zheng Shou. Show-1: Marrying pixel and latent diffusion models for text-to-video generation. *arXiv preprint arXiv:2309.15818*, 2023. 2

[90] Lvmin Zhang and Maneesh Agrawala. Packing input frame context in next-frame prediction models for video generation. *arXiv preprint arXiv:2504.12626*, 2025. 2

[91] Richard Zhang, Phillip Isola, Alexei A Efros, Eli Shechtman, and Oliver Wang. The unreasonable effectiveness of deep features as a perceptual metric. In *Proceedings of the IEEE conference on computer vision and pattern recognition*, pages 586–595, 2018. 2

[92] Yinan Zhang, Eric Tzeng, Yilun Du, and Dmitry Kislyuk. Large-scale reinforcement learning for diffusion models. In *European Conference on Computer Vision*, pages 1–17. Springer, 2024. 2

[93] Canyu Zhao, Mingyu Liu, Wen Wang, Weihua Chen, Fan Wang, Hao Chen, Bo Zhang, and Chunhua Shen. Moviedreamer: Hierarchical generation for coherent long visual sequence. *arXiv preprint arXiv:2407.16655*, 2024. 2

[94] Zikai Zhou, Shitong Shao, Lichen Bai, Shufei Zhang, Zhiqiang Xu, Bo Han, and Zeke Xie. Golden noise for diffusion models: A learning framework. *arXiv preprint arXiv:2411.09502*, 2024. 2, 3, 4

# AutoRefiner: Improving Autoregressive Video Diffusion Models via Reflective Refinement over the Stochastic Sampling Path

## Supplementary Material

### A. Details on DMD Loss and Samplers

We provide additional details on the formulation of the step-distillation objective using DMD loss, along with descriptions of the corresponding stochastic and deterministic sampling procedures discussed in Sec. 3.3 of the main paper.

**Detailed Formulation of DMD Loss.** Following previous works [78, 87], the gradient of reverse KL divergence in Eq. (5) of the main paper is obtained by

$$\begin{aligned} & \nabla_{\theta} \mathcal{L}_{\text{DMD}} \\ &= \mathbb{E}_t (\nabla_{\theta} \text{KL} (q_{\theta, t} (\mathbf{x}_t) \| p_t (\mathbf{x}_t))) \\ &= \mathbb{E}_t \left( \nabla_{\theta} \left( \mathbb{E}_{\mathbf{x}_t \sim p_{t|0}(\mathbf{x}_t|\mathbf{x}), \mathbf{x} \sim q_{\theta}(\mathbf{x})} \log \left( \frac{q_{\theta, t} (\mathbf{x}_t)}{p_t (\mathbf{x}_t)} \right) \right) \right) \\ &= \mathbb{E}_{t, \mathbf{x}_t \sim p_{t|0}(\mathbf{x}_t|\mathbf{x}), \mathbf{x} \sim q_{\theta}(\mathbf{x})} [s_{\text{fake}} (\mathbf{x}_t, t) - s_{\text{real}} (\mathbf{x}_t, t)] \frac{d\mathbf{x}_t}{d\theta}, \end{aligned} \quad (11)$$

where sampling from the conditional  $p_{t|0}$  corresponds to the forward diffusion process in Eq. (4) of the main paper. In practice, the samples from the model distribution  $q_{\theta} (\mathbf{x})$  are obtained autoregressively as

$$q_{\theta} (\mathbf{x}_t) = q_{\theta} (\mathbf{x}_t^{1:N}) = \prod_{i=1}^N q_{\theta} (\mathbf{x}_t^i | \mathbf{x}_t^{<i}). \quad (12)$$

$s_{\text{fake}}$  and  $s_{\text{real}}$  are score functions for the model distribution and real-data distribution, i.e.,

$$\begin{aligned} s_{\text{fake}} (\mathbf{x}_t, t) &= \nabla_{\mathbf{x}_t} \log q_{\theta} (\mathbf{x}_t), \\ s_{\text{real}} (\mathbf{x}_t, t) &= \nabla_{\mathbf{x}_t} \log p (\mathbf{x}_t). \end{aligned} \quad (13)$$

**Few-step stochastic sampling.** Both base AR-VDMs used in our method—Self-Forcing and CausVid are step-distilled from a standard multi-step bidirectional video diffusion model [71] that follows the training objective of Rectified Flows [42, 44], with which the forward diffusion schedule is defined as

$$\mathbf{x}_t = t\mathbf{x}_0 + (1-t)\mathbf{x}_{T_{\text{max}}}. \quad (14)$$

This constitutes a ground truth velocity field of

$$\mathbf{v}_t = \frac{d\mathbf{x}_t}{dt} = \mathbf{x}_0 - \mathbf{x}_{T_{\text{max}}}, \quad (15)$$

with which the training objective is defined as mean squared error (MSE) between ground truth velocity and predicted velocity from a flow-based model  $\mathbf{v}_{\theta_0}$

$$\mathcal{L}_{\text{flow}} = \mathbb{E}_{\mathbf{x}_0, \mathbf{x}_{T_{\text{max}}}, t} \|\mathbf{v}_{\theta_0} (\mathbf{x}_t, t) - \mathbf{v}_t\|^2. \quad (16)$$

Fine-tuned based on the model  $\mathbf{v}_{\theta_0}$ , a denoising prediction step of Self-Forcing and CausVid in Eq. (3) of the main paper is parameterized in a form similar to Tweedie's estimation [16, 55]

$$\begin{aligned} \mathbf{x}_{0|t_j}^i &= G_{\theta} \left( \mathbf{x}_{t_j}^i; \mathbf{x}^{<i}, t_j \right) \\ &= \mathbf{x}_{t_j}^i + (1-t_j) \mathbf{v}_{\theta} \left( \mathbf{x}_{t_j}^i; \mathbf{x}^{<i}, t_j \right), \end{aligned} \quad (17)$$

where  $\mathbf{v}_{\theta}$  shares the same architecture as  $\mathbf{v}_{\theta_0}$ .  $\mathbf{v}_{\theta}$  replaces bidirectional attention masks with causal attention masks in self-attention layers, which in turn enables the use of KV cache to condition on historical frames  $\mathbf{x}^{<i}$ .

**Implementation of ODE-based sampling.** For the example of ODE sampling in Fig. 3 of the main paper. We change a stochastic sampling step of

$$f_{\theta, t_j} \left( \mathbf{x}_{t_j}^i \right) = \Psi \left( \mathbf{x}_{0|t_j}^i, \epsilon_{j-1}^i, t_{j-1} \right), \quad (18)$$

to the following

$$\tilde{f}_{\theta, t_j} \left( \mathbf{x}_{t_j}^i \right) = \mathbf{x}_{t_j}^i + (t_{j-1} - t_j) \mathbf{v}_{\theta} \left( \mathbf{x}_{t_j}^i; \mathbf{x}^{<i}, t_j \right), \quad (19)$$

which is the same ODE sampling schedule used by the base bidirectional model  $\mathbf{v}_{\theta_0}$ .

### B. Implementation Details

We provide more implementation details on our used base AR-VDMs and training configurations.

**Base AR-VDMs.** Our used base AR-VDMs—Self-Forcing and CausVid are both distilled from the bidirectional 1.3B Wan2.1 [71] model. Self-Forcing is distilled to generate a video chunk using four denoising steps  $\{1000, 750, 500, 250\}$ . CausVid is distilled to generate a video chunk using three denoising steps  $\{1000, 757, 522\}$ . Both models generate a total of 21 latent frame videos with 3-frame chunks generated at each autoregressive rollout, which are decoded into 81-frame videos at a spatial resolution of  $480 \times 832$  by a 3D VAE [71].

**Training Details.** For training with DMD loss, we use an AdamW [45] optimizer with a learning rate  $1 \times 10^{-4}$ . For the score functions in Eq. (13), we adopt a Wan2.1-14B model as the real score function and a Wan2.1-1.3B

	<b>Total Score <math>\uparrow</math></b>	<b>Quality Score <math>\uparrow</math></b>	Subject Consist. $\uparrow$	Background Consist. $\uparrow$	Aesthetic Score $\uparrow$	Imaging Quality $\uparrow$	Temporal Flicker $\uparrow$	Motion Smooth. $\uparrow$	Dynamic Degree $\uparrow$
Self-Forcing [32]	84.05	84.93	95.02	96.39	65.78	69.24	99.11	98.42	69.44
+LoRA	82.10	82.65	93.17	92.96	63.90	66.64	95.43	96.42	95.83
+InitNoiseRefiner	83.76	84.63	94.41	95.79	65.19	68.78	99.01	98.26	72.22
+AutoRefiner (ours)	<b>84.72</b>	<b>85.41</b>	95.42	96.17	65.84	69.33	99.09	98.24	76.39
CausVid [88]	83.06	84.24	96.24	95.83	64.71	68.33	99.41	98.07	63.89
+LoRA	83.43	84.74	94.97	95.14	62.50	71.65	97.48	97.27	88.89
+InitNoiseRefiner	82.23	83.13	96.50	96.74	65.18	67.68	99.53	98.31	44.44
+AutoRefiner (ours)	<b>83.84</b>	<b>84.82</b>	95.55	95.86	65.13	69.10	99.25	98.36	69.44
	<b>Semantic Score <math>\uparrow</math></b>	Object Class $\uparrow$	Multiple Objects $\uparrow$	Color $\uparrow$	Spatial Relation $\uparrow$	Scene $\uparrow$	Temporal Style $\uparrow$	Overall Consistency $\uparrow$	Human Action $\uparrow$
Self-Forcing [32]	80.54	94.22	88.41	86.81	81.24	52.83	24.58	26.80	97
+LoRA	79.93	90.90	83.08	88.11	78.92	56.32	24.93	27.08	96
+InitNoiseRefiner	80.29	92.17	86.51	85.72	82.71	53.78	24.49	27.05	97
+AutoRefiner (ours)	<b>81.95</b>	93.83	88.64	88.99	86.56	57.20	24.59	26.71	98
CausVid [88]	78.35	94.22	88.03	86.46	74.04	48.47	23.93	25.77	96
+LoRA	78.18	89.95	82.62	86.00	73.32	58.79	24.31	25.93	91
+InitNoiseRefiner	78.64	93.83	87.27	88.16	76.44	46.95	23.72	25.68	97
+AutoRefiner (ours)	<b>79.93</b>	95.25	86.43	89.78	79.30	53.05	23.91	26.21	97

Table 5. VBench results across all 16 evaluation dimensions for comparison with baseline methods using DMD loss as objective.

model as the fake score function. For training with reward scores, we use an AdamW optimizer with a learning rate of  $2 \times 10^{-5}$ . The reward weights are set to 0.25, 0.1 and 0.1 for InternVideo2, HPSv2.1 and CLIP, respectively. Among the 81 generated frames, we randomly sample 2 frames to compute image reward scores, and extract 4-frame clips with a sampling interval of 10 frames to compute video reward scores. Following the configurations of the base models, we use a classifier-free guidance (CFG) [24] scale of 3.0 for Self-Forcing and 3.5 for CausVid. The timestep shift [17] is set to 5.0 for Self-Forcing and 8.0 for CausVid. We apply  $L_2$  regularization for reward-based training and not for DMD loss-based training, as the reverse-KL formulation of the DMD loss in Eq. (11) inherently regularizes the noise refiner by keeping its tilted distribution close to the base model distribution. We set both LoRA rank and alpha as 128. All trainings are performed on 8 H100 GPUs with a valid batch size of 48 for 1,000 iterations, taking roughly 24 hours to complete. We use fully shared data parallel (FSDP) and gradient checkpointing to reduce the maximum GPU memory usage.

## C. Further Quantitative Results

We provide additional quantitative evaluations, including full VBench scores across all dimensions, an ablation study on the LoRA rank, and a comparison of how different training-based methods influence the sample diversity and dynamic degree of the base AR-VDM.

**Full VBench Scores.** We provide in Tab. 5 the full VBench scores across all 16 dimensions corresponding to

the main comparison results reported in Tab. 1 of the main paper, including 7 quality-related metrics and 9 semantic-related metrics.

**Ablation On LoRA rank.** We report the ablation results for different LoRA ranks in Tab. 6.

LoRA Rank	Quality Score $\uparrow$	Semantic Score $\uparrow$	Total Score $\uparrow$
16	84.97	<b>82.00</b>	84.38
32	84.72	80.93	83.97
64	84.93	81.52	84.25
128	<b>85.41</b>	81.95	<b>84.72</b>

Table 6. Ablation on different LoRA ranks.

**Diversity & Dynamic Preservation.** We further analyze how reward-based training with different methods impacts the sample diversity and dynamic degree of the base AR-VDM using image similarity metrics. For each method, we generate 10 videos using different random seeds for each of 70 text prompts. Sample diversity is computed as the average cosine similarity between the embeddings of all video pairs generated from the same prompt, where each video embedding is obtained by averaging its frame-level DINO [48] embedding. Dynamic degree is evaluated by the similarity between temporally neighboring frames within each video using LPIPS [91], SSIM [77] and PSNR [29], with a sampling interval of 5 frames. The results are reported in Tab. 7. We observe that, while LoRA exhibits mode-collapse behavior reflected by significantly increased DINO similarity, *AutoRefiner* preserves a sample diversity

comparable to the base model. Moreover, both LoRA and InitNoiseRefiner substantially degrade the dynamic degree—showing increased similarity in LPIPS, SSIM, and PSNR scores relative to the base model—whereas *AutoRefiner* consistently improves these metrics.

Method	Diversity		Dynamic Degree	
	DINO $\downarrow$	LPIPS $\uparrow$	SSIM $\downarrow$	PSNR $\downarrow$
Self-Forcing [32]	.8577	.1359	.5636	17.52
+InitNoiseRefiner	.8394	.0652	.6807	19.47
+LoRA	.9039	.0488	.7430	19.32
+AutoRefiner (ours)	.8597	.1758	.4393	14.25

Table 7. Comparison of sample diversity and dynamic degree using frame-wise similarity metrics after reward-based training.

## D. Further Qualitative Results

We present additional qualitative comparisons with baseline methods, including DMD-based training using Self-Forcing as the base model (Fig. 9), DMD-based training using CausVid as the base model (Fig. 10), and reward-based training using Self-Forcing as the base model (Fig. 11). In Fig. 8, we illustrate the two reward hacking behaviors of training an initial noise refiner for AR-VDMs—motion degradation and ‘grid-like’ artifacts, as discussed in Sec. 3.3 of the main paper. Please refer to the HTML file in the supplementary materials to review the videos for all examples presented in both the main paper and the appendix.



Figure 8. An illustration of two reward-hacking issues arising in initial noise refinement: static motion (as in the “firework” example) and “grid-like” artifacts (as in the “money” example).

## E. Subjective Evaluation

We conduct a subjective evaluation with 10 participants to compare *AutoRefiner* with several baseline methods. Each method generates videos for 10 text prompts. Participants are asked to watch each video together with its corresponding prompt and rate the overall video quality on a 1–5 scale

(where higher ratings indicate better quality). During evaluation, participants are instructed to consider the following criteria:

- **Visual Quality:** How clear, realistic, and artifact-free the generated video appears.
- **Temporal Naturalness & Consistency:** How smooth and coherent the motion is across frames.
- **Semantic Alignment:** How well the video content corresponds to the meaning of the text prompt.

The results are reported in Tab. 8.

	User preference score $\uparrow$
Self-Forcing [32]	2.23
+InitNoiseRefiner	2.31
+LoRA	2.25
+AutoRefiner (ours)	3.69

Table 8. Comparison with baseline methods with subjective evaluation on a 1–5 scale.

## F. Future Work

Future work may extend the idea of noise refinement with self-reflection to further mitigate the exposure bias issue in frame extrapolation tasks, which is one of the core challenges in autoregressive generation for continuous data. We already observe such potential when applying *AutoRefiner* to CausVid, as reflected by the reduced color-drifting artifacts in Fig. 6 (main paper) and Fig. 10. Another promising direction is to explore higher-level motion controllability with a noise refiner, such as controlling the speed or camera motion of generated videos, by steering the sampled noises. For image generation, future work may also investigate applying the concept of pathwise noise refinement to text-to-image models step-distilled by DMD or Consistency Distillation [36, 64], enabling downstream improvements such as reward alignment or enhanced physical soundness.



Figure 9. More qualitative comparison with baselines on training with DMD loss, using Self-Forcing [32] as the base model. *AutoRefiner* alleviates visual artifacts (left example), and improves motion alignment with text prompt (right example) compared to the base model.

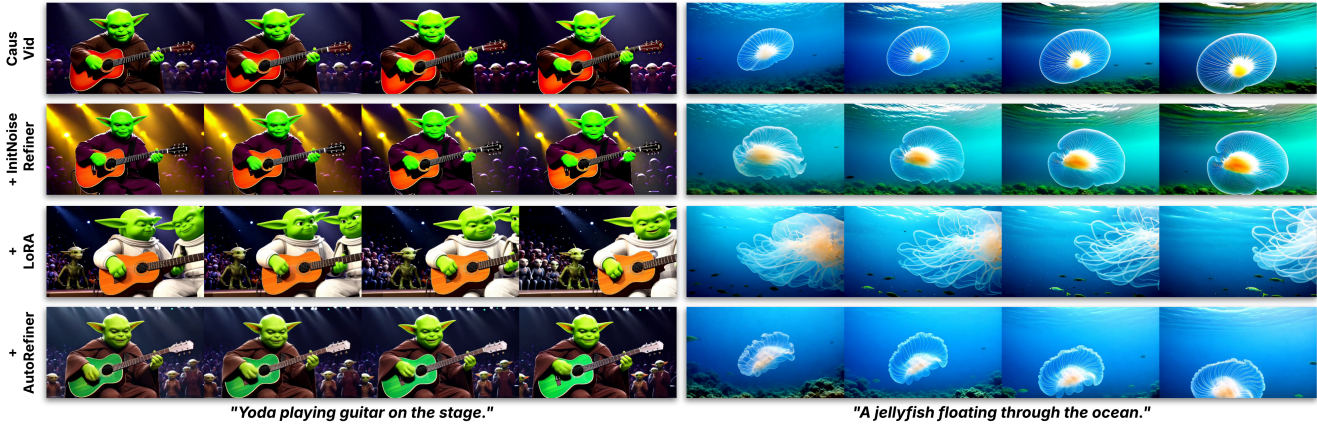


Figure 10. More qualitative comparison with baselines on training with DMD loss, using CausVid [88] as the base model. *AutoRefiner* alleviates the cross-frame inconsistency issue of CausVid, as observed in the gradually saturated color of “Yoda” (left) and “ocean” (right).



Figure 11. More qualitative comparison with baselines on training with reward scores. *AutoRefiner* demonstrates smoother temporal transitions (left example) and generates motion that appears more natural and dynamic than the baselines (right example).